IEEE Open Journal of
Ultrasonics, Ferroelectrics, and Frequency Control

Received 23 April 2021; revised 27 July 2021 and 7 September 2021; accepted 8 October 2021.
Date of publication 15 October 2021; date of current version 2 November 2021.

Digital Object Identifier 10.1109/OJUFFC.2021.3120234

Fluid Independent Flow Determination by Surface Acoustic Wave Driven Ultrasonic Techniques

ANDREAS HEFELE[1,2], CHRISTOPH STROBL[2], ERIK BAIGAR[3], GEORG KURZMAIER[2], ALEXANDER REINER[1], ANDREAS L. HÖRNER[1], AND ACHIM WIXFORTH[1] (Member, IEEE)

[1]Institut für Physik, Universität Augsburg, 86159 Augsburg, Germany
[2]Thermo Fisher Scientific, 82110 Germering, Germany
[3]Thorlabs GmbH, 85232 Bergkirchen, Germany

CORRESPONDING AUTHOR: ANDREAS HEFELE (andreas-hefele@gmx.de)

This work was supported by Thermo Fisher Scientific.

ABSTRACT A fluid-independent ultrasonic approach for flow determination in microchannels in the harsh environment of an ultra high pressure liquid chromatography (UHPLC) system is presented. Ultrasonic waves in the fluid are excited by separate media surface acoustic waves (SAW) of Rayleigh-Wave type. The $LiNbO_3$ SAW chip being equipped with interdigitated transducers for SAW excitation also marks the bottom of the fluid channel and thus allows for very effective SAW coupling to the fluid. The channel ceiling acts as an acoustical mirror for longitudinal ultrasonic waves propagating through the fluid. To deduce the fluid flow from the ultrasonic transmission after reflection, we employ a combination of time differential phase and time of flight measurements with a two port vector network analyzer. To verify and assign our experimental results, we use an adapted time explicit finite element method. In the simulation, both the piezoelectric single crystal and the fluid are included and we solve the linear Navier-Stokes equation to evaluate the background flow. By changing the ultrasonic propagation direction, we are able to deduce the fluid volume flow over time with very high accuracy, independent of the actual liquid in the channel.

INDEX TERMS Surface acoustic wave (SAW), flow sensor, fluid flow measurement, high performance liquid chromatography (HPLC), ultrasonic, substrates, $LiNbO_3$.

I. INTRODUCTION

IN MICROSYSTEMS, where small amounts of fluids are propagating within tiny channels, the flow properties of the fluids are very difficult to monitor and investigate. In this work, the flow measurement is investigated with a special focus to high performance liquid chromatography (HPLC).

In high performance liquid chromatography, a so called mobile phase or eluent consist of liquid solvents, is provided by a high pressure pump. A sample to be tested (constituent) is then injected inside the fluidic path and pumped through the HPLC column. The interaction of the stationary phase, the mobile phase and the constituents causes the constituents to flow with different speeds through the column. The stationary phases consist of porously arranged microparticles inside the column with polar adhesive molecular ends (normal phase chromatography) or in the case of the more common reverse phase chromatography with added nonpolar particles (e.g. C_{18} chains). For the detection of the temporal separated constituents downstream the column, a special detector like for example an UV VIS detector or a mass spectrometer is used. The peak like detector signals are recorded and sampled in a so called chromatogram. Among other important properties, like the pressure or the temperature in the system, also the fluid flow itself is an important property. A feedback loop to control the pump could, for example, improve the constant flow through the system. To monitor and record the process parameters like the fluid flow or other properties, is extremely important where regular quality control is indispensable. The medical field is a suitable example.

There are some established technics to measure flow inside tubes or other geometries of flow channels like rectangular channels. Measurement schemes like differential pressure technics [1] or Coriolis flow sensors [2] are common. Also Thermal flow sensors [3] or optical methods [4] have been used. Ultrasonic sensors [5], either based on the Doppler effect or on a time of flight measurement approach are also

usual methods in flow determination. Generally, all of these sensors are material dependent and therefore require more or less complex methods to compensate for fluid properties like, e.g. temperature or pressure variations.

To overcome most of the problems of the established flow systems, we are using an ultrasonic high frequency technique on a chip. Our sensor is based on a SAW (surface acoustic wave) driven ultrasonic time of flight measurement. Fluid sensors based on SAW have attracted more and more attention in recent years [6], [7], [8]. So far, it is common to use a piezoelectric SAW-substrate supporting shear waves which exhibit only very little interaction with the flowing fluid. An example for such a substrate is $LiTaO_3$ 36° YX. Such shear wave sensors generally relate on a flow dependent renormalization of the SAW propagation velocity c_s due to the mass loading or conductivity changes of the sensing layer in contact with the sensitive surface of a substrate. Also, some reports regarding flow sensing with SAW have been published [9]–[11]. These sensors, however, are based on direct SAW (mostly Shear Waves) resonance frequency shifts caused by flow dependent pressure or temperature shifts. They operate in the range of flows between 10 ml/min and 1000 ml/min with a corresponding significantly lower need in accuracy than our application with a maximum of 2-3 ml/min.

In contrast to such more common approaches, our work presented in this article is based on bulk waves in the fluid being excited by the strong interaction with Rayleigh type SAW [12], [13]. A comprehensive overview of sensors using leaky Rayleigh Waves in the last decades can be found in [7]. There, first approaches in the eighties and nineties of the last century were used to measure, e. g., liquid density and viscosity [14]. Later, flexural plate (or Lamb) waves [15] were used to simultaneously measure various characteristics of various fluids [16], [17]. Also, conventional applications of a flexural plate (or Lamb) wave sensor to measure flow with a ultrasonic transit time approach have been reported [18]. Lamb waves are guided waves inside a thin plate, that meets the condition $h_p \leq \lambda_F$. Where h_p is the thickness of the plate and λ_F is the fluid wavelength. The A0 wave mode for example is deflected antisymmetrically at both sides of the plate. Thus, if only one side is excited by a transducer, the other side will act as an emitter as well. Therefore, waves can be produced inside a channel, without a transducer that comes into direct contact with the fluid. However, for the sake of high frequencies and therefore short wavelengths, which result in higher resolution, the wall for plate modes would become too thin to yield a mechanically robust flow sensor. Therefore, we chose to directly use a (leaky) Rayleigh Waves substrate.

Here, we employ three transducers on one chip (see Fig. 1) to compensate fluid properties at the flow measurement. The use of SAW to excite the ultrasonic waves enables to use relatively small channels ($\sim$ 0.5 mm^2 cross section area), because of the high frequencies that are possible with SAW. Conventional transit flow meters have a maximum frequency of about 8 MHz [19]. The use of higher frequencies

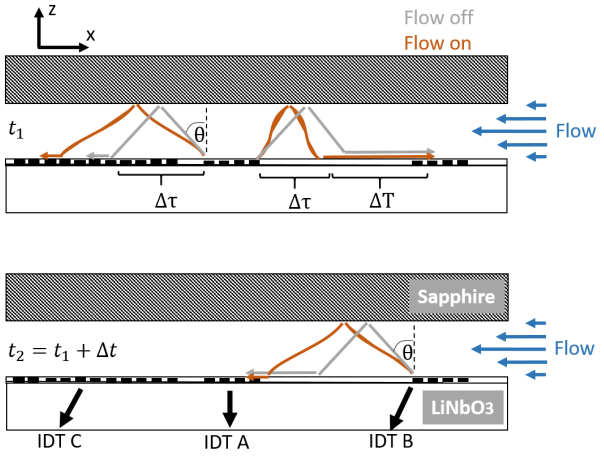

FIGURE 1. Schematic of the measurement cell at two different times with and without flow. The acoustic path with background flow "on" is represented by orange arrows. The grey arrows indicate the acoustic path without flow. At t = t1 the central IDT (A) is the emitter and the right IDT (B) and left transducers (C) are the receivers. At t = t2 the sending and receiving properties of the small IDTs (A,B) are reversed. For the center IDT (A), we make use of its bidirectional characteristic to enable "time of flight" and phase differential measurement simultaneously. $\Delta\tau$ is the propagation time of the wave, if it hits directly the receiving IDT. The propagation needs an additional time ΔT if the wavepulse hits not directly the receiving IDT. In general, this is the case with the shorter IDTs. The long IDT is designed in a way, that with various speed of sound c_F in the fluids, the wavepulse always directly meets the long IDT. Therefore it is possible to measure the flow independent of fluid. The additional flow dependent time differences, indicated by the bended arrows, are small compared to the propagation time. So this time difference could be neglected in terms of the propagation measurements.

gives us the opportunity to excite non dispersive plane wave pressure modes inside the channel, because the height H of the channel meets the condition $H \gg \lambda$. λ is the wavelength of the ultrasonic waves inside the fluid. Employing the conventional, lower frequency approaches, would result in highly dispersive guided waves [20], [21] in our small channel in the flow direction. Our time of flight measurement is indirectly carried out by a SAW phase measurement. The sensitivity of the phase measurement is linearly dependent on the frequency which allows for a very precise indirect measurement of the transit time difference, as stated above. For the flow measurement, we have the waves propagate through the channel, reflect them at its ceiling and re-convert it back into SAW on the very same piezoelectric chip, as seen in Figs 1 and 9. The flow dependent changes of the SAW propagation parameters are then used to directly measure the fluid flow.

For the measurement, a time differential phase approach, using a vector network analyzer (VNA) and an external switch array, has been developed. We measure flow rates up to 2 ml/min with an absolute error of 1 to 10 μl/min. For a single fluid flow measurement, this corresponds to a flow speed

(cross sectional average) accuracy of 40 to 400 μm/s with a maximum flow speed of 9 cm/s. We therefore have a range of the relative error from 0.1 % (Water at 2 ml/min) to 1.5 % (Acetonitrile at 0.1 ml/min). Additionally, the combination of a differential phase measurements and a time of flight measurement, using a third IDT reveals the possibility to do the flow measurement independent of the actual fluid used. Here, as we will point out below, an accuracy of 20 μl/min (0.8 mm/s) in the laminar fluid regime is reached. The somewhat larger standard error in this case can be explained with the continuous fluid property change and with a significantly higher error of the dwell time measurement with the network analyzer used for the measurement in this work, compared to the pure phase measurement.

II. THEORY

The transition between the solid bound SAW and the bulk wave in the fluid is not an immediate step, but is represented by a transition where constantly the same relative amount of wave energy is transmitted into the fluid. This leads to the fact that a continuous SAW, for example, entering the liquid becomes exponentially attenuated over time. Such waves are called leaky SAW waves and are described in [22] and [23].

To result in an effective SAW transmission into the fluid, a non negligible part of the SAW mode must be polarized normal to the substrate of the surface. Then, it becomes possible to excite pressure waves inside the fluid. Such a mode with a large part of the particle displacement and thus of the wave energy being oriented normal to the substrate surface is the mentioned Rayleigh-Wave. The sensor presented in this work hence consists of a single $LiNbO_3$ YX 128° SAW chip, representing both the sensing part and additionally acting as the bottom of the fluid channel. The $LiNbO_3$ chip is covered with a thin inert fused SiO_2 layer to protect the IDTs from mechanical and chemical influences of the fluid. Because the thickness of the SiO_2 layer is only a very small fraction of the fluid- or SAW-wavelength, the wave properties are practically not changed compared with a chip that is directly in contact with the fluid. The channel walls provides the sealing functionality and the top of the channel is made of a sapphire plate to ensure best acoustic reflection properties (Figs 1, 2 and 5).

As schematically depicted in Fig. 1, the ultrasonic wave in our setup becomes spatially shifted by a flowing fluid as compared to the propagation of the wave without flow. The orange bent arrows in the sketch indicate a shift being proportional to the flow velocity inside the channel. Generally, however, the flow velocity is a function of the position normal to the flow direction. In the simplest case, this dependence yields a parabolic shape (Hagen Poiseuille flow).

Assuming the flow velocity v_x is simply given by its constant mean value within the whole channel at a fixed time:

$$v_x = Q/A. \tag{1}$$

Here, Q is the volume flux and A denotes the area of the channel cross section. For explaining the basic principle we

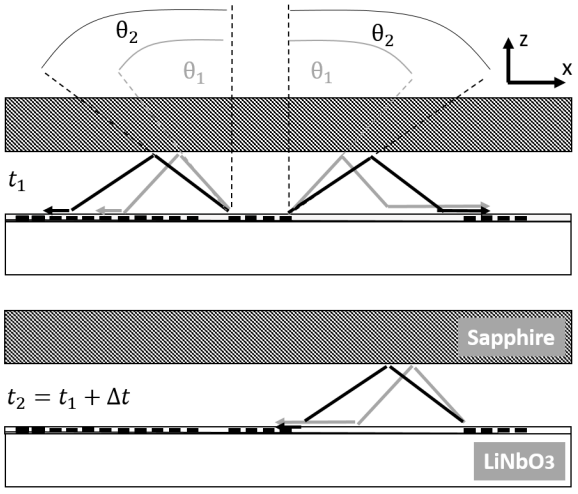

FIGURE 2. Acoustic paths for two different fluids. The different Rayleigh-angles $\Theta = \sin^{-1}(\frac{c_F}{c_S})$ are due to the different sound velocities c_F, here chosen to $c_F(\Theta_2) > c_F(\Theta_1)$. At $t = t_1$ the central IDT is the emitter. The bidirectional nature of a conventional single-split-IDT is thus deliberately employed to measure the pure dwell time $\Delta\tau$ (residence time of the sound wave) in the fluid at every second time step. At $t = t_2$ the two identical IDTs exchange their sending and receiving roles.

first look at two transducers, A and B located on the bottom of this fluidic channel (Fig. 1, both right transducers). Assuming that a wave packet is excited at time $t = t_1$ by IDT A which travels from IDT A to IDT B (positive $\times$ direction) through the fluid. We define the time $t_2 = t_1 + \Delta t$, such that the electrical cross talk, the leaky SAW pulse (substrate), the pressure wave pulse (fluid) and also a few following echo pulses are considered to have been already received by the other IDTs. Hence, after $t = t_2$, the received signal is back at the baseline again.

An absolute phase determination, as will be explained in detail in section 3 reveals the phase $\varphi_{AB}(t_1)$ of the pressure wave pulse in the fluid. This $\varphi_{AB}(t_1)$ is stored in a shift register for later access. At $t = t_2$, the transmitting (tx) and receiving (rx) characteristic of IDT A and B are exchanged. Now, the wave packet is excited by IDT B and thus propagates towards negative x direction. After reception of all relevant signals by IDT A, the corresponding phase $\varphi_{BA}(t_2)$ is obtained. If Δt is considered to be small, then we get:

$$\varphi_{AB} - \varphi_{BA} = f(v_x, \Delta\tau). \tag{2}$$

Here, $\Delta\tau$ denotes the dwell- or residence time of the pressure pulse within the fluid. If the receiving ITD is relatively small, as it is the case with IDT A and B, we measure an additional time $\Delta T(c_f)$ in an extended dwell time

$$\Delta\tau'(c_f) = \Delta\tau(c_f) + \Delta T(c_f), \tag{3}$$

where the wave propagates as SAW again (see Fig. 1, upper right pathway of the sound wave). Hence, we later introduced a third long ITD that measures the dwell time for all possible relevant Rayleigh angles and corresponding speed of sound

inside the fluid to a good approximation. In the following, the important function $f\,(v_x, \Delta\tau)$ is calculated. We start with the spatial shift of a pulse propagating from IDT A to IDT B caused by the flow in the negative x direction during the dwell time $\Delta\tau$. Under the above assumption of a constant flow velocity and flow profile, we get the simple expression

$$\Delta x_{AB} = v_x \Delta\tau \left(c_f\right). \tag{4}$$

Here, we assume the wave being only spatially shifted while residing inside the fluid. This Δx can by the way also be expressed in terms of the SAW velocity c_s because the pressure wave after reflection at the channel ceiling couples back into the SAW substrate, exhibiting a slight spatial shift with respect to the directly transmitted SAW, as it is depicted in Fig. 1.

Then, the apparent path of the SAW is

$$\Delta x_{AB}\,(t) = c_s \Delta t_s + f(s_i). \tag{5}$$

Δt_s is the apparent temporal delay of the SAW due to the spatial shift Δx of the wave in the fluid and $f\,(s_i)$ is a function containing all symmetrical shifts related to the flow and its direction. That could for example be the pressure- or temperature dependent variation of the signal. Fortunately, all signals being related to the flow dependent shift are symmetrical according to the definition above. Hence, any unwanted signals can be treated relatively simply. The propagation time $\Delta\tau'$ changes due to the flow and due to symmetrical shifts $f\,(s_i)$. We denote this term t_{AB} and get:

$$t_{AB} = \Delta\tau' - \Delta t_s - f\,(s_i)\,/c_s \tag{6}$$

whereas $\Delta t_s = v_x \Delta\tau / c_s$. t_{AB}, as usual and to compare it with our measurement, can also be expressed by a correspondent phase $\varphi = 2\pi \mathrm{t_{AB}} f$:

$$\varphi_{AB} = 2\pi f(\Delta\tau' - v_x \Delta\tau / c_s - f\,(s_i)\,/c_s). \tag{7}$$

If we now look at the opposite wave propagation direction from IDT B to IDT A at the second time Interval starting at t_2, we obtain a spatial shift Δx_{BA} in the positive x direction n and correspondingly a phase φ_{BA} :

$$\varphi_{BA} = 2\pi f(\Delta\tau' + v_x \Delta\tau / c_s - f\,(s_i)\,/c_s). \tag{8}$$

Assuming small changes of the fluid properties after the time Δt, needed for signal acquisition, the phase φ_{AB} and φ_{BA} can now be subtracted to compensate for the term including $f\,(s_i)$:

$$\Delta\varphi = \varphi_{BA} - \varphi_{AB} = \frac{4\pi f v_x \Delta\tau}{c_s}. \tag{9}$$

Here, $\omega = 2\pi f$ is the angular frequency and ω / c_s is the SAW wave vector k. Then it results in:

$$\Delta\varphi = 2k v_x \Delta\tau \tag{10}$$

To yield this phase difference to additionally be independent of a specific fluid (i) one has to also measure the dwell time $\Delta\tau(i)$ which for a given channel geometry relates to the specific sound velocity c_{Fi}. Hence we arrive at the final equation:

$$\frac{\Delta\varphi}{\Delta\tau} = 2k v_x. \tag{11}$$

This term is constant as a function of a constant flow velocity v_x, if the SAW wave vector $k = f / c_s$ can assumed to be a constant. Then, as the measurement is done at a fixed frequency, only the changes of the SAW velocity c_s are relevant. Because the Rayleigh SAW velocity of $LiNbO_3$ YX 128° is relatively sensitive to temperature variations, and to check for the temperature influence on our measurements, we construct a worst case estimation: In this scenario, we assume a very large temperature change of the fluid, being in direct contact with the chip surface. We therefore use the temperature dependent properties of $LiNbO_3$ YX128° with a thin layer of SiO_2 as, e.g., being published in [24]. We thus assume a temperature dependent velocity change of 50ppm/°C at the chip surface. Even with a pretended very large temperature shift of $\Delta T = 50$ °C, we arrive at an estimated relative maximum error of only about 0.2% for the relevant signal (equation (11)). This small error would then be caused by the temperature dependent change of the wave vector. Therefore, we feel safe to consider k to be constant, which is necessary for a constant flow signal. It should be noted, that during a real measurement, the temperature shifts are definitely much smaller than in this worst case scenario.

For the first, high accuracy single fluid measurements as shown in Fig. 3, the fluid independency is not necessary. Hence, in this measurements, we can omit the third IDT C. For the fluid independent measurements (Fig. 6), however, IDT C is needed and thus used to measure the pure dwell time $\Delta\tau$.

Therefore, we now consider the wave being emitted from IDT A under the Rayleigh angle $\theta_i = sin^{-1} c_{Fi} / c_s$ and then, after being reflected at the channel ceiling reaching the long transducer IDT C. This process is schematically depicted in Fig. 2. To ensure that the reflected wave packet actually hits IDT C, its necessary length and position with respect to IDT A is thus dictated by the possible ranges of Rayleigh angles $\theta_i = sin^{-1} c_{Fi} / c_s$ for a variety of fluids and given channel height. We were able to show theoretically the possibility to measure the flow not only independent of temperature and pressure variations inside the fluid channel, but also independent of all other liquid properties at a very good approximation.

III. EXPERIMENTAL SETUP AND MEASUREMENT

Our flow cell (Fig. 5) is connected with a conventional UHPLC System of Thermo Fisher Scientific. The schematic of the whole system can be seen in Fig. 7. The delivering of defined various fluids and the flow control is performed by a UHPLC integrated Piston Pump System of type Vanquish VF-P10. As stated above, the substrate of choice for the flow cell is a $LiNbO_3$ rot 128° single Crystal chip covered with a thin 200 nm fused SiO_2 layer. Employing standard

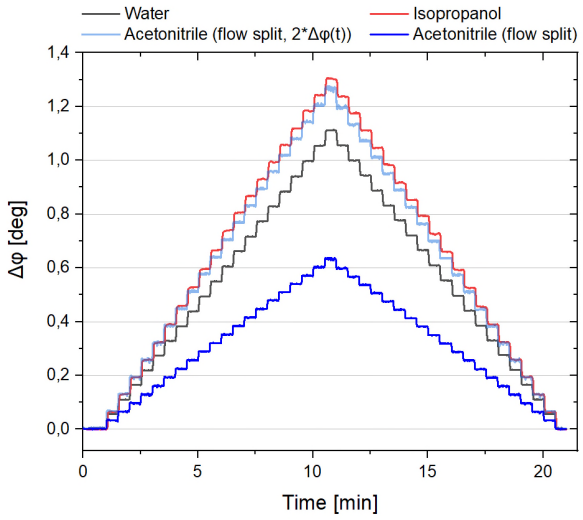

FIGURE 3. Compensated phase difference measurements for various increasing and decreasing flow rates (in steps of ΔQ = 0.1 ml/min) and for three different liquids (water, isopropanol and acetonitrile). The investigated flow range is 0-2 ml/min. Because of an assumed laminar- to 'disturbed laminar' flow regime for the acetonitrile at approximately 1.4 ml/min, a flow splitter (50:50 of volume) has been used to show the whole flow range in the laminar regime. For the sake of completeness: The measured flow dependent phase shift for the highly viscous acetonitrile is multiplied by two which makes the data visually comparable to the other liquids.

photolithography and subsequent thermal or e-beam metallization, the IDTs were deposited before the deposition of SiO_2 cap layer. The IDTs were designed to result in a wavelength of $\lambda_S = 59\ \mu$m corresponding to a SAW frequency of 68 MHz for the given substrate. This frequency was chosen because for higher frequencies the attenuation of the ultrasonic wave inside the fluid becomes too strong and therefore the received signal power became too small to achieve proper rx signals. The attenuation length (1/e) of the f = 68 MHz pressure wave in water at $T = 20°C$ is roughly 8 mm [25]. With a channel height of 0.5 mm and the 6 mm extension of the IDT along the propagation direction (Fig. 1), the choice of the operating frequency is a crucial tradeoff, because on the other hand, as shown in equation (9), the sensitivity of course also rises with increasing frequency.

After excitation at the IDT, the SAW is converted into a bulk wave in the fluid under the Rayleigh angle θ and after reflection at the channel ceiling again travels back to the surface. The waves on the left side couple directly into the long IDT (C) and are therefore directly converted into an electrical, detectable signal. The waves propagating initially to the right side, however, hit the SAW chip surface somewhere between the two IDTs. Because of the symmetry of the problem, they are re-converted into a piezomechanic SAW before they reach IDT (B) as such and where they are subsequently detected as an electrical signal. As being explained above, at $t_2 = t_1 + \Delta t$, the center (A) and the right IDT (B) exchange their *tx* (sending-) and *rx* (receiving-) roles. The transmission and receiving part of the experiment is carried out using the two port vector network analyzer being directly connected to a switch array, in order to change *tx* and *rx* of the IDTs (Fig. 7).

The relevant signal to be measured and evaluated is the phase of the scattering parameters S21 and S12 representing the system transfer function and therefore the relative vectorial part of the transmitted and received waves. For an overview, we plot the various relevant S-parameters in Fig. 10. The S21 and S12 signals measured with IDT A (port 1) and IDT B or C (port 2) as receiver are nearly symmetrical. Therefore, we chose to only just show the S21 parameter. The used VNA is of monodirectional type, with a fixed tx and rf port. The required periodical changes of the measurement directions (S21 <> S12) is hence done by two external switches, being triggered by the VNA after each sweep. With this equipment and setup, a sweep time down to $\Delta t = 20$ ms over a frequency range (total bandwidth) of 20 MHz, with an IF bandwidth of 10 kHz, could be safely secured. Transmitting signal level was +0 dBm. The received power of the relevant signal peaks were in the range between -23 dBm and -32 dBm. For each sweep, the time gate method was used by transforming the detected signal into the time domain. This way, unwanted (and spurious) signals like the above mentioned electromagnetic crosstalk and remaining leaky SAW signals can be eliminated due to their different propagation times. An additional switching step makes the simultaneous measurement of the wave traveling from the center ITD (A) to the left IDT (C) possible. Here, too, the signal is transformed into the time domain and the maximum of the relevant wave pulse is tracked to carry out the crucial time of flight $\Delta\tau$. The resolution of this approach is limited by the Fourier transform characteristics of the time resolution ($\Delta t_{min} \approx 1/\Delta f = 50$ns), where Δf is the frequency range of the measurement.

The changes of the fluid properties, especially the speed of sound c_F of the fluid, cause very large phase shifts as compared to the smaller flow dependent phase changes. It is intuitively understandable that any change of c_F changes the Rayleigh angle and therefore, in turn, acoustic rays, or acoustic pulses, with different Rayleigh angles can also described by different thicknesses of the fluid layer between the SAW chip and the sapphire channel ceiling. (c.f. Fig. 2). This, in turn, strongly affects the dwell time for each measurement which can be directly seen in Fig. 4, where we have shown a continuous one side measurement of the phase of S21 or S12 for various concentrations of ethanol and acetonitrile in water. The relation of the phases due to the varying speed of sound can be clearly seen. The maxima of the curves are the points with maximum c_F and therefore maximum Rayleigh angle θ. In Fig. 4, also the correspondent magnitude of the transmission signal is depicted. The plot shows a typical result for water / alcohol mixtures with a viscosity maximum between the pure fluid values [26]. In terms of the amplitude measurement of the transmission signal S21, this results in a maximum absorption of the acoustic wave at maximum

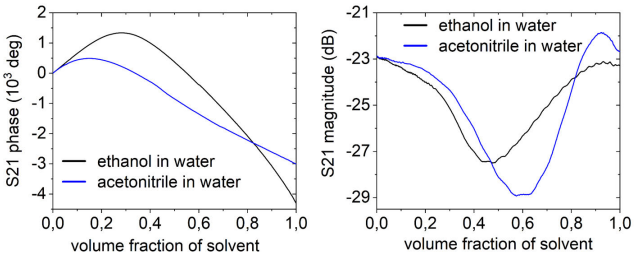

FIGURE 4. Measured variation of the transmission signal S21(phase and magnitude) at fixed maximum frequency (68 MHz) caused by a variation of ethanol (black) and acetonitrile (blue) concentrations in pure water. An external flow would have practically non influence on this signals because the phase variation due to the flow is too small as compared to the phase variation due to the liquid properties (especially the variation of the speed of sound) on this scale.

viscosity and therefore minimum transmission. The plot in Fig. 4 shows the large variability of the transmission signal caused by the varying fluid properties of the alcohol/water mixtures. Therefore, we used these fluid mixtures to deal with a worst case estimate for our fluid independent flow measurement. Possible temperature and pressure variations might also vary the relevant fluid properties like the speed of sound c_F or the viscosity. However, the variations due to the different fluid mixtures are significantly higher and therefore we believe it is sufficient to show any fluid independency by only varying the mixture.

Fig. 3 shows the measured representation of equation (10) for pure phases of water, isopropanol and acetonitrile. For this measurement, we only used IDT A and IDT B (see Fig. 1) and continuously changed their rx and tx role after each measurement. We show this measurement especially because of the high accuracy for the single fluid flow as being obtained in non-gradient flow measurements. Without IDT C for measuring the real dwell time $\Delta\tau$ and normalizing the phase difference signal with this time, these first measurements are still not fluid-independent. Normalization of the measured signal to apparent dwell time $\Delta\tau' = \Delta\tau + \Delta T$, would still not give a fluid-independent signal has been explained above.

If for some reason like for example a higher channel or a longer chip, any pressure wave pulses are reflected more than once (n times), we need to multiply equation (9) or (10) with n, leading to:

$$\Delta\varphi = 2nkv_x\Delta\tau \tag{12}$$

In our case, n is an integer number $0 < n \leq 2$.

In this section, we now are interested in the best signal with respect to the standard error: We thus use the second pulse for measuring the phase difference in water and acetonitrile (Fig. 3). This was the pulse with the largest signal in water (see Fig. 10). Therefore $n = 2$ in equation (12). For isopropanol, we used the signal pulse which propagates only once through the channel ($n = 1$). The fluid handling part of the UHPLC system was set to deliver predefined discrete

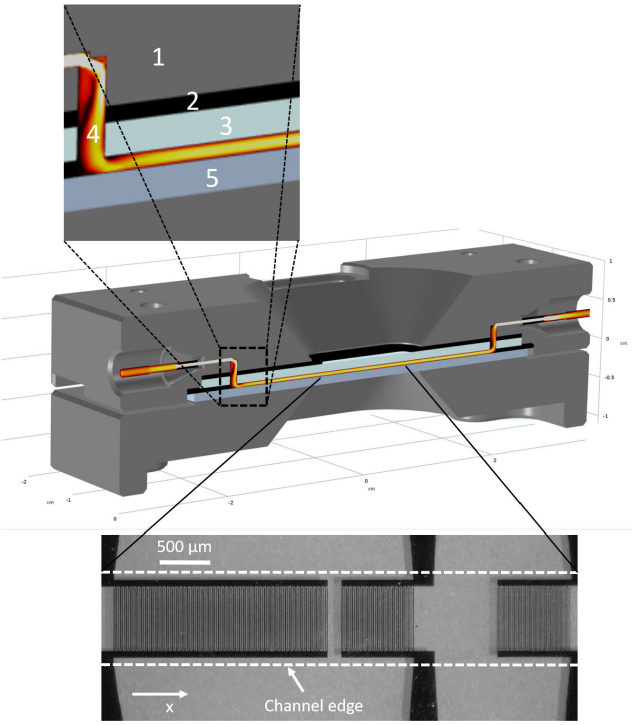

FIGURE 5. Cross sectional representation of the flow cell. The functional parts of the cell are sandwiched between two steel blocks (1) where the upper part contains the lateral fluidic connections. The SAW chip (5) is mounted inside a recessed frame of the lower steel block. Directly on top of the chip, a carbon reinforced Teflon seal (thickness 0.5 mm) forms the channel-wall (2). The channel top consists of a thin sapphire plate (3) on top of which an additional sealing layer (2) is mounted. It is thus possible to inspect the inside of the channel with a microscope to check, for example, for turbulences. This specific construction is designed to withstand pressures up to 5 MPa. An identical cell without the "viewing window" can endure > 50 MPa. The IDT (lower picture) consists of single split IDT-Gold fingers (thickness: 50 nm, Finger width: $\lambda/4 \sim 15\mu m$. f = 68 MHz) directly on the LiNbO3 substrate and is covered with 200 nm SiO2. The IDTs on the right side are identical and consist of 17 finger pairs whereas the longer left IDT holds 60 finger pairs.

flow steps of $\Delta Q = 0.1$ ml/min and keep each of these set flow values for 30 s until we reached a total flow of 2 ml/min. Then, following the same steps, we decreased the flow back to zero. It can be clearly seen that the lower the speed of sound for a given fluid, the higher the phase sensitivity because the waves remaining longer inside the fluid and thus becomes more shifted. This simple fact, namely the linear dependence of the phase shift $\Delta\varphi$ with respect to the dwell time $\Delta\tau$ could already be seen in equation (10).

For the measurements as being depicted in Fig. 6, we used all three IDT as explained above and hence result in a fluid-independent flow measurement by adding an additional third switching step to measure the dwell time $\Delta\tau$. Here, too, considered a single pass of the pressure wave for all fluids and mixtures ($n = 1$ in eq. 12). This finally yielded a reliable way to eliminate the fluid properties from our measurements as

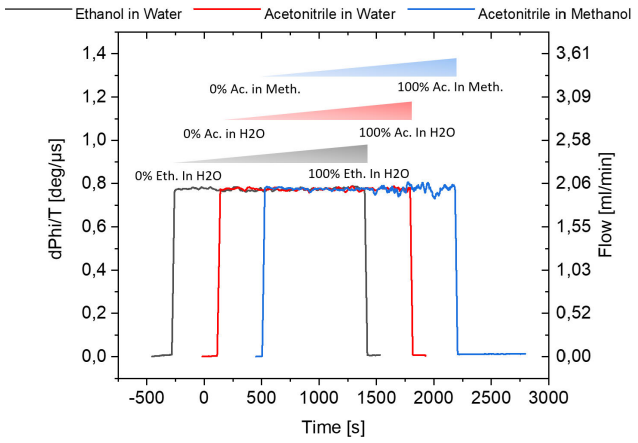

FIGURE 6. **Flow measurement with three different liquids and liquid mixtures as indicated above the traces. A few seconds after beginning the measurement, the flow was switched on from 0 to 2 ml/min and the measured phase shift divided by the simultaneously measured dwell time is recorded. Remarkably, the signals remain constant for all investigated fluids and mixtures. The measurement uncertainty remains roughly around as low as ± 20 μl/min in the laminar regime. At about 70 % acetonitrile in methanol and above, however, the noisiness of the signals increases noticeably up to 150 μl/min, most likely being caused by a laminar-to turbulent transition of the fluid flow due to the low viscosity and density of especially acetonitrile.**

TABLE 1. **Acoustic properties of constituents used for the flow measurement in Figure 6, at 25°C [27], [28].**

	Water	Ethanol	Methanol	Acetonitrile
$c_f[m/s]$	1497	1145	1104	1260
$\eta[mPa\ s]$	0.890	1.082	0.545	0.344

shown in equation (11). In Fig. 6, and as a proof, we thus show three different flow measurements for three different continuously changing liquid mixtures in our system, where we deliberately change the fluid composition and thus the sound velocity and viscosity during the measurement. Starting from zero flow, the flux was then abruptly increased up to $Q = 2$ ml/min but with a simultaneous and continuous intermixing of fluid B into fluid A. This intermixing $A_{1-x} - > B_x$ is sketched in the upper part of the Fig. 6 for the three fluid mixtures. The acoustic properties of the used constituents are in Table 1. Notably, within a few percent of a ml/min, no influence of the type of fluid or mixture can be detected in the flow dependent measurements, although during the experiments, the viscosities and the sound velocities are being considerably changed.

The comparatively small 'noisy' signatures in the data may in part be explained by the dynamic intermixing procedure itself, mostly being caused by the quite drastic (local) changes of the viscosity during the measurement.

IV. SIMULATION

For the modeling of our experimental findings we made use of the COMSOL Multiphysics [29] packages. The simulation environment is two dimensional and is mainly composed of

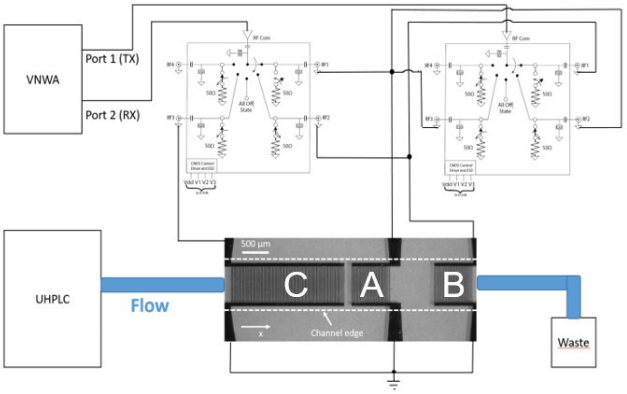

FIGURE 7. **Sketch of the setup: The fluid handling system is based on a commercial UHPLC system. It delivers a constant flow and the possibility to handle and process at least two fluids. Attached to the UHPLC is our measurement flow cell with the SAW-Chip and a fluid waste outlet. The rf signal processing is done employing a two Port Vector Network analyzer (VNA). Two external switches take care of the time differential, bidirectional phase measurements and the determination of the dwell time of the pressure wave within the fluid. The switches and the VNA are controlled via PC (not shown).**

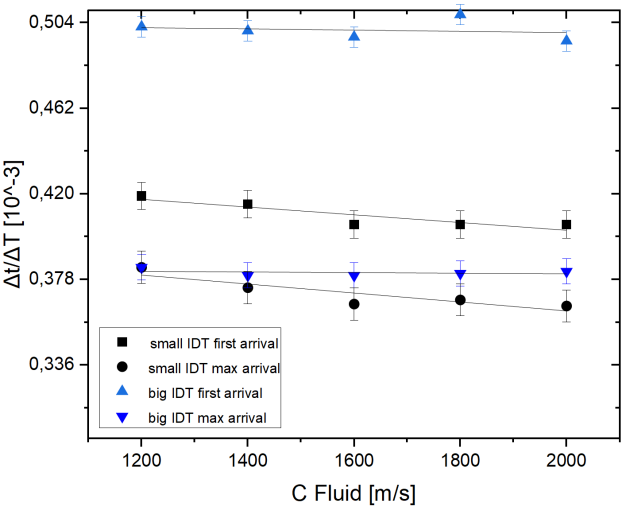

FIGURE 8. **Flow dependent temporal shift of the wave divided by the dwell time received at IDT B (black) and the IDT C (blue) for various c_f. Circles and inverted triangles indicates a tracking of the maximum of the wave in the time domain and triangles/ squares indicates tracking of first appearance of the wave in the time domain. The overall flow velocity is 1 m/s.**

a piezoelectric solid state ($LiNbO_3$) and a fluid domain to solve the linear Navier Stokes equation. The fluid domain is connected to the $LiNbO_3$ substrate via a thin fused SiO_2 layer. Boundary treatment is based on acoustic impedance considerations to simulate only the reflective part of the wave but not the transmitted part. The linear Navier Stokes equation is solved in first-order perturbation around the background steady-state variables (p_0, T_0, $\boldsymbol{u_0}$, ρ_0), which define the background flow. The perturbations (p, T, $\boldsymbol{u}$, p) in this case, are mainly caused by the acoustic waves and are considered

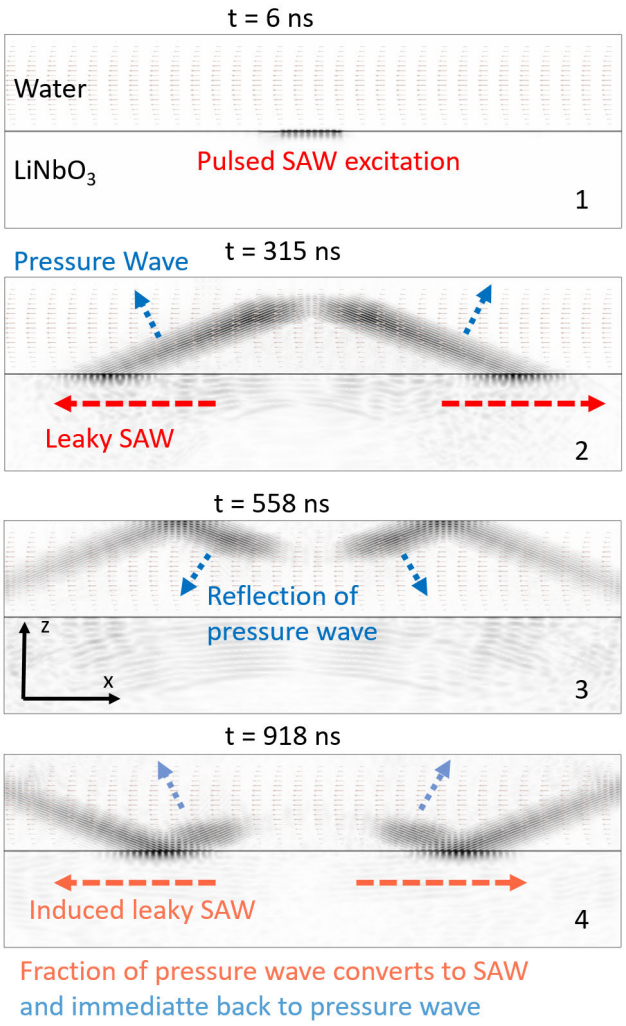

FIGURE 9. **Four different snapshots of the graphical representation of the time domain simulation. Each picture shows the LiNbO3 chip (below) and the fluid domain (above) at a specific point in time. The pulsed leaky SAW excitation can be seen in the first picture. In the second image, the main part of the SAW is converted into pressure waves that propagate bidirectionally into a negative and positive flow direction. The remaining leaky SAW is also clearly visible. In picture three, parts of the wave were reflected at the channel top and heading back to the SAW surface. Picture 4 shows the first conversion of pressure waves back into SAW and, due to their leakage behavior, an immediate conversion back into pressure waves. During the propagation time, all wave packets within the fluid become slightly shifted in the negative x-direction due to the background flow within the fluid channel.**

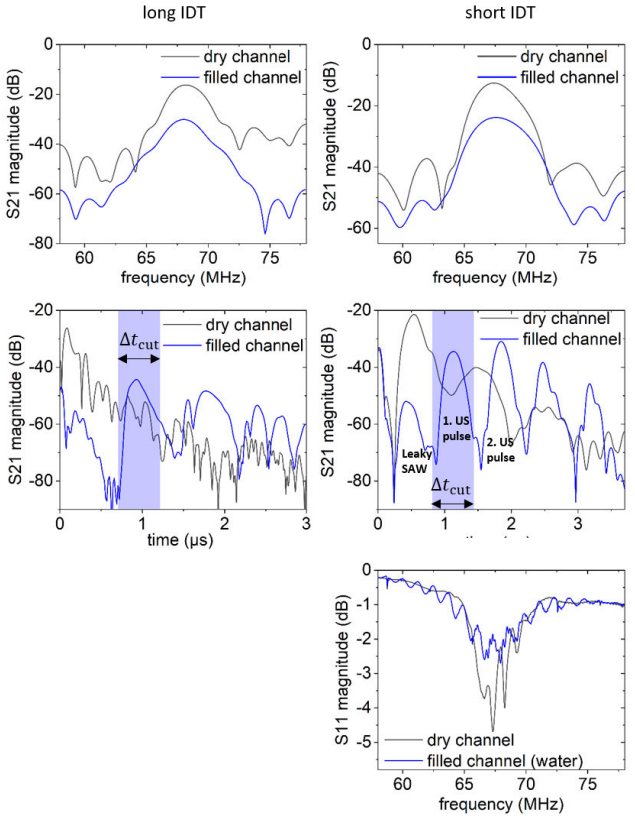

FIGURE 10. **Overview of some S-parameters of the long IDT (left) and the short IDT (right). The transmission spectrum in the frequency domain (top) contains just the relevant signal peaks of the time domain. The specific signal peak used for the measurement is highlighted by a blue transparent bar in the time domain. The blue graphs represent the signals with fluid (here exemplary water) inside the channel and the gray plot is the transmitted signal with no fluid inside the channel. The transmission signals S21 and S12 are nearly identical (not shown), due to the symmetry of each delayline. Therefore, we actually just plotted only the S-parameter in one direction, defined with IDT A as the transmitter (port1) and IDT B or C (port 2) as a receiver. On the bottom right, the S11 signal of the short IDT with and without fluid is shown.**

to be small and thus having only perturbative influence on the parabolic background flow. A time dependent study is performed to solve the flow behavior of the system within the first $\sim$ 1150 ns after a pulsed electrical SAW excitation $\Delta t_{ex} = n/f$ of the central IDT (see Fig. 9). Here, n denotes the number of fingers, and f the SAW frequency. This short electrical excitation causes the above mentioned bidirectional excitation of the leaky SAW. Looking at Fig. 9, the wave transmission inside the fluid domain and therefore the attenuation of the SAW is clearly seen. After a reflection at the channel ceiling, the waves are traveling back to the $LiNbO_3$ chip. Here, because of the total symmetry of the problem, they are re-converted into a Rayleigh SAW mode at the chip surface. Also, the immediate back conversion into the pressure wave is visible. The mean electrical potential is in the first case measured at the rx IDT B. This way, it is possible to detect a voltage as a function of time.

The first step was to validate the simulation for a given fluid (water, $T = 22°C \rightarrow c_F = 1489m/s$) with 16 different flow velocities form -67 mm/s to 67 mm/s. This corresponds to a volume flow of -1.5 ml/min – 1.5 ml/min given a channel of H $\times$ W $=$ 0.5 mm $\times$ 0.75 mm. The measurement itself is extended to a flow rate up to 2 ml/min. To calculate the flow dependent shift of the SAW, equation (10) is used.

To calculate the dwell time, the triangle formed by Rayleigh angle and the channel is considered. The corresponding phase difference is hence

$$\Delta\varphi = \frac{8\pi v_x f H}{c_F \sqrt{(c_S^2 - c_F^2)}}. \tag{13}$$

Being calculated for two different c_f, corresponding to two different temperatures in pure water [30] the comparison shows that calculated, measured and simulated data are very similar.

The second step is to also consider the long ''dwell time'' IDT C and then divide the phase signal (here expressed in terms of a time shift) by the rx dwell time at the short and the long IDT. The first arrival of the wave comes actually closest to the calculated dwell time $\Delta\tau$. However, as the maximum of the dwell time is easier to access, both values are considered and compared in Fig. 8. As can be seen, the tracked signals at the dwell time IDT are constant and fluid independency can be shown also with the simulated environment. The decrease of the tracked signal at the small IDT can be explained by a reduction of the distance, the acoustic wave has to travel as a SAW after coupling into the substrate again as depicted in Fig. 9.

V. CONCLUSION

We presented a novel approach to measure the fluid-independent flow in the environments of an ultra high pressure liquid chromatography (UHPLC) system. We here employ a triple IDT arrangement on a piezoelectric $LiNbO_3$ substrate for Rayleigh surface acoustic wave and analyze the rf signals using a two port vector network analyzer and an external switch array to enable bidirectional measurements. To start with, we presented the experimental part of the work by showing a very accurate flow (up to 2 ml/min) dependent measurement with a simple two IDT arrangement. We used three different single phase fluids to illustrate the phase difference measurements being linear to the flow inside the channel. In the second, experimental part, we finally employed a third, long IDT and by adding an additional time step to the measurement we were able to measure the real dwell time. This dwell time was then used to correct the measured phase signal and finally extracting a flow signal being independent of the type of fluid inside the channel. Moreover, in an additional demonstration experiment, we continuously changed the fluid properties inside the channel in order to create a measurement environment that comes close to the situation inside a HPLC system with constant eluent gradients. Our experimental findings are very well supported by a two dimensional finite element simulation.

ACKNOWLEDGMENT

The authors thank the Technical Team of the University of Augsburg. They would also like to thank everyone who has contributed to this work in various ways.

REFERENCES

[1] S. B. M. Beck and J. Mazille, ''A study of a pressure differential flow meter that is insensitive to inlet conditions,'' *Flow Meas. Instrum.*, vol. 12, nos. 5–6, pp. 379–384, Jan. 2002, doi: 10.1016/S0955-5986(01)00034-6.

[2] T. Wang and R. Baker, ''Coriolis flowmeters: A review of developments over the past 20 years, and an assessment of the state of the art and likely future directions,'' *Flow Meas. Instrum.*, vol. 40, pp. 99–123, Dec. 2014, doi: 10.1016/j.flowmeasinst.2014.08.015.

[3] J. T. W. Kuo, L. Yu, and E. Meng, ''Micromachined thermal flow sensors—A review,'' *Micromachines*, vol. 3, no. 3, pp. 550–573, Mar. 2012, doi: 10.3390/mi3030550.

[4] G. M. Quénot, J. Pakleza, and T. A. Kowalewski, ''Particle image velocimetry with optical flow,'' *Exp. Fluids*, vol. 25, no. 3, pp. 177–189, 1998, doi: 10.1007/s003480050222.

[5] P. Hauptmann, N. Hoppe, and A. Püttmer, ''Application of ultrasonic sensors in the process industry,'' *Meas. Sci. Technol.*, vol. 13, no. 8, pp. R73–R83, Aug. 2002, doi: 10.1088/0957-0233/13/8/201.

[6] D. B. Go, M. Z. Atashbar, Z. Ramshani, and H.-C. Chang, ''Surface acoustic wave devices for chemical sensing and microfluidics: A review and perspective,'' *Anal. Methods*, vol. 9, no. 28, pp. 4112–4134, 2017, doi: 10.1039/c7ay00690j.

[7] G. Lindner, ''Sensors and actuators based on surface acoustic waves propagating along solid–liquid interfaces,'' *J. Phys. D, Appl. Phys.*, vol. 41, no. 12, Jun. 2008, Art. no. 123002, doi: 10.1088/0022-3727/41/12/123002.

[8] M. S. Brugger, L. G. Schnitzler, T. Nieberle, A. Wixforth, and C. Westerhausen, ''Shear-horizontal surface acoustic wave sensor for non-invasive monitoring of dynamic cell spreading and attachment in wound healing assays,'' *Biosensors Bioelectron.*, vol. 173, Feb. 2021, Art. no. 112807, doi: 10.1016/j.bios.2020.112807.

[9] Y. Wang, Z. Li, L. Qin, M. K. Chyu, and Q.-M. Wang, ''Surface acoustic wave flow sensor,'' in *Proc. Joint Conf. IEEE Int. Freq. Control Eur. Freq. Time Forum (FCS)*, May 2011, doi: 10.1109/FCS.2011.5977735.

[10] S. G. Joshi, ''Flow sensors based on surface acoustic waves,'' *Sens. Actuators A Phys.*, vol. 44, no. 3, pp. 191–197, Sep. 1994, doi: 10.1016/0924-4247(94)00804-3.

[11] T. Nomura, A. Saitoh, and K. Koyama, ''Mass flow sensor using dual SAW device,'' in *Proc. IEEE Int. Freq. Control Symp. Joint with 21st Eur. Freq. Time Forum*, May 2007, pp. 25–30, doi: 10.1109/FREQ.2007.4319023.

[12] L. Rayleigh, ''On waves propagated along the plane surface of an elastic solid,'' *Proc. London Math. Soc.*, vols. 1–17, no. 1, pp. 4–11, Nov. 1885, doi: 10.1112/plms/s1-17.1.4.

[13] A. Wixforth, C. Strobl, C. Gauer, A. Toegl, J. Scriba, and Z. V. Guttenberg, ''Acoustic manipulation of small droplets,'' *Anal. Bioanal. Chem.*, vol. 379, nos. 7–8, pp. 982–991, Aug. 2004, doi: 10.1007/s00216-004-2693-z.

[14] T. Nomura, M. Takebayashi, S. Furukawa, and M. Obana, ''Surface acoustic wave sensor for sensing acoustic properties of liquid,'' in *Proc. IEEE Ultrason. Symposium Int.*, vol. 1, Nov. 1995, pp. 547–550, doi: 10.1109/ultsym.1995.495637.

[15] H. Lamb, ''On waves in an elastic plate,'' *Proc. R. Soc. Lond. A, Containing Papers Math. Phys. Character*, vol. 93, no. 648, pp. 114–128, Mar. 1917, doi: 10.1098/RSPA.1917.0008.

[16] F. B. Cegla, ''Measurement of bulk velocity and attenuation in fluids and particle suspensions using the quasi-scholte mode,'' in *Proc. AIP Conf.*, 2006, vol. 820, no. 1, pp. 1245–1252, doi: 10.1063/1.2184667.

[17] G. Lindner *et al.*, ''P5G-2 acoustic surface wave induced propagation of liquids in open channels,'' in *Proc. IEEE Ultrason. Symp.*, Oct. 2007, pp. 2331–2334, doi: 10.1109/ULTSYM.2007.586.

[18] S. C. Y. Fuchs, Y. Hoog, and B. Koenig, ''Fluid metering,'' U.S. 2019 03 31 642 A1, Feb. 16, 2021.

[19] G. Rajita and N. Mandal, ''Review on transit time ultrasonic flowmeter,'' in *Proc. 2nd Int. Conf. Control, Instrum., Energy Commun. (CIEC)*, Jan. 2016, pp. 88–92, doi: 10.1109/CIEC.2016.7513740.

[20] (Accessed: Mar. 31, 2021). *Elastic Waves in Solids I—Free and Guided Propagation | Daniel Royer | Springer*. [Online]. Available: https://www.springer.com/de/book/9783540659327?gclid=CjwKCAjwu5CDBhB9EiwA0w6sLQiFV28x-59d-NhLOFbaGte_QIZ8BX9-1pObphByoNkLjWUTAhozHBoChrcQAvD_BwE

[21] J. L. Rose, ''Guided wave nuances for ultrasonic nondestructive evaluation,'' *IEEE Trans. Ultrason., Ferroelectr., Freq. Control*, vol. 47, no. 3, pp. 575–583, May 2000, doi: 10.1109/58.842044.

[22] T. A. Franke and A. Wixforth, ''Microfluidics for miniaturized laboratories on a chip,'' *ChemPhysChem*, vol. 9, no. 15, pp. 2140–2156, Oct. 2008, doi: 10.1002/cphc.200800349.

[23] C. Strobl, "Mikro-und Nanofluidik auf piezoelektrischen Substraten," Ph.D. dissertation, Fakultät Physik, LMU München, Munich, Germany, 2005, p. 157.
[24] M. Tomar, V. Gupta, and K. Sreenivas, "Temperature coefficient of elastic constants of SiO_2 over-layer on $LiNbO_3$ for a temperature stable SAW device," *J. Phys. D, Appl. Phys.*, vol. 36, no. 15, p. 1773, Jul. 2003, doi: 10.1088/0022-3727/36/15/304.
[25] T. D. Rossing and T. D. Rossing, "Springer handbook of acoustics," *Choice Rev. Online*, vol. 45, no. 5, pp. 45-2674–45-2674, 2008, doi: 10.5860/choice.45-2674.
[26] F. Franks and D. J. G. Ives, "The structural properties of alcohol–water mixtures," *Q. Rev. Chem. Soc.*, vol. 20, no. 1, pp. 1–44, 1966, doi: 10.1039/QR9662000001.
[27] B. González, A. Domínguez, and J. Tojo, "Dynamic viscosities, densities, and speed of sound and derived properties of the binary systems acetic acid with water, methanol, ethanol, ethyl acetate and methyl acetate at T=(293.15, 298.15, and 303.15) K at atmospheric pressure," *J. Chem. Eng. Data*, vol. 49, no. 6, pp. 1590–1596, 2004, doi: 10.1021/je0342825.
[28] M. N. Roy, B. K. Sarkar, and R. Chanda, "Viscosity, density, and speed of sound for the binary mixtures of formamide with 2-methoxyethanol, acetophenone, acetonitrile, 1, 2-dimethoxyethane, and dimethylsulfoxide at different temperatures," *J. Chem. Eng. Data*, vol. 52, no. 5, pp. 1630–1637, 2007, doi: 10.1021/je700026d.
[29] *Comsol Multiphysics V. 5.4*, Comsol, Stockholm, Sweden, 2018. [Online]. Available: http://www.comsol.com
[30] W. Marczak, "Water as a standard in the measurements of speed of sound in liquids," *J. Acoust. Soc. Amer.*, vol. 102, no. 5, pp. 2776–2779, Nov. 1997, doi: 10.1121/1.420332.

ANDREAS HEFELE received the B.Sc. degree in lab on a chip topics in 2016 and the M.Sc. degree in physics regarding microfluidics and SAW sensors in HPLC applications in 2018. He is currently pursuing the Ph.D. degree with the Chair of Prof. Wixforth as a part of a cooperational project between the University of Augsburg and Thermo Fisher Scientific, Germering.

CHRISTOPH STROBL received the Ph.D. degree in physics from the Ludwig-Maximilians-Universität, Munich, Germany, in 2005. He worked in the field of micro- and nanofluidics with SAW devices. Since 2005, he has been working as a Senior Scientist at Thermo Fisher Scientific, develops HPLC and UHPLC pumps and focus on handling thermal effects and mixing of liquids in HPLC pumps.

ERIK BAIGAR graduated in physics at LMU, Munich, in 1995. He received the Ph.D. degree in physics for spectroscopic studies on ultrafast electron transfer reactions, dynamic Stokes shift and wave packet dynamics in 2003. Thereafter, he worked one year at the Institute of Soil Ecology, Helmholtz Centre, Munich, on dissolved organic matter before returning to LMU for work on ultrashort laser physics and femtochemistry. In parallel, he joined Olympus BioSystems in 2001 designing optical equipment for TIRF-, fluorescence-, and live cell imaging. In 2007, he started working at the Liquid Chromatography Division, Thermo Fisher Scientific, Germering, developing high performance absorption and fluorescence spectrometers, also collaborating with external contractors on novel detection technology. Since 2019, he has been working at the Spectroscopy Group, Thorlabs GmbH, Bergkirchen, in the field of coded aperture-based Raman spectroscopy.

GEORG KURZMAIER received the degree in precision engineering from the Fachhochschule, Munich, in 1980. After that, he joined the Micrography Branch of the Agfa Gaevert AG, Munich, where he was working on opto-mechanical design and also was involved in series introduction and maintaining quality. In 1993, he switched to working on digital printing and scanning devices at Agfa Gaevert AG before joining Dionex Softron AG in 2007. He was responsible for the opto-mechanical design and system integration of a variety of HPLC detector instruments (absorption and fluorescence quantitation of liquids) and the related accessories, including flow cells before he retired in 2020.

ALEXANDER REINER was born in 1987. He received the B.Sc. degree in physics in 2012 and the M.Sc. degree in Augsburg in 2014. He is currently pursuing the Ph.D. degree with the University of Augsburg on multiparametric gas sensing using metal organic frameworks in combination with surface acoustic waves. Prior to his studies, he finished a training as an industrial mechanic. Before, he worked for one and a half year at the Helmholtz Zentrum, Munich, on automating single cell sampling and PCR, including robotics and lab-on-a-chip technologies.

ANDREAS L. HÖRNER was born in Eichstätt, Germany, in 1976. He received the Diploma degree in physics from the University of Munich, and the Ph.D. degree in physics from the University of Augsburg. Since 2006, he leads the Solid State Nanosystems Group with the Chair of Prof. Wixforth in Augsburg. His main research topics are sensors and actuators using surface acoustic waves.

ACHIM WIXFORTH (Member, IEEE) received the degree in physics from the University of Hamburg in 1984 and the Ph.D. degree in 1987.

Thereafter, he spent a post-doctoral period at the University of California at Santa Barbara (UCSB), where he focused on MBE growth of layered semiconductor quantum systems. After ten years at LMU, Munich, Germany, he moved to Augsburg in 2002. He is currently the Chair for experimental physics I at the University of Augsburg, Germany. There, he studies biophysical effects on membranes, single biopolymers, and living cells. This development has led to the foundation of a very successful startup company in 2000 which has been acquired first by Olympus Life and Materials Science and later by Beckman-Coulter, an U.S.-based leader in diagnostics. He has authored and coauthored more than 220 scientific articles, most of them in prestigious journals (H-index 49). He is an inventor of about 25 patents worldwide. His research interests are the deliberate modification and analysis of matter on the nano scale. These include solid state-based nano systems, such as semiconductor quantum films, wires and quantum dots and their electronic, optical, and mechanical properties but also hybrid systems with his specialty being surface acoustic waves. He was a recipient of many important awards during his career. These include the Walter-Schottky Prize for solid state research in 1998, the Bavarian Innovation Award for the Advalytix-Technology in 2001, the Best Bavarian Small Business Award in 2002, the BioTrends Award in 2003, and the IEEE C. B. Sawyer Memorial Award in 2011.